Data in Brief 53 (2024) 110140

Contents lists available at ScienceDirect

Data in Brief

journal homepage: www.elsevier.com/locate/dib

Data Article

A collection of 157 individual neuromelanin-sensitive images accompanied by non-linear neuromelanin-sensitive atlas and a probabilistic locus coeruleus atlas

Tae-Ho Lee[a,d,*], Sun Hyung Kim[b,*], Joshua Neal[a], Benjamin Katz[c,d], Il Hwan Kim[e]

[a] Department of Psychology, Virginia Tech, USA
[b] Department of Psychiatry, University of North Carolina, Chapel Hill, USA
[c] Department of Human Development and Family Science, Virginia Tech, USA
[d] School of Neuroscience, Virginia Tech, USA
[e] Department of Anatomy and Neurobiology, University of Tennessee Health Science Center, USA

ARTICLE INFO

Article history:
Received 22 December 2023
Revised 19 January 2024
Accepted 25 January 2024
Available online 1 February 2024

Dataset link: 157 neuromelanin-sensitive image dataset (age: 8 - 64yrs) (Original data)

Keywords:
Neuromelanin-sensitivity image
Locus Coeruleus (LC) probability atlas
Non-linear neuromelanin-sensitive atlas
Multi-atlas-based majority voting

ABSTRACT

The current dataset aims to support and enhance the research reliability of neuromelanin regions in the brainstem, such as locus coeruleus (LC), by offering raw neuromelanin-sensitive images. The dataset includes raw neuromelanin-sensitive images from 157 healthy individuals (8–64 years old). In addition, leveraging individual neuromelanin-sensitive images, a non-linear neuromelanin-sensitive atlas, generated through an iterative warping process, is included to tackle the common challenge of a limited field of view in neuromelanin-sensitive images. Finally, the dataset encompasses a probabilistic LC atlas generated through a majority voting approach with pre-existing multiple atlas-based segmentations. This process entails warping pre-existing atlases onto individual spaces and identifying voxels with a majority consensus of over 50 % across the atlases. This LC probabilistic atlas can minimize uncertainty variance associated with choosing a specific single atlas.

* Corresponding authors.
E-mail addresses: taehol@vt.edu (T.-H. Lee), sunhyung_kim@med.unc.edu (S.H. Kim).

https://doi.org/10.1016/j.dib.2024.110140

Specifications Table

Subject	Neuroscience
Specific subject area	Cognitive Neuroscience
Data format	Raw, Defaced
Type of data	NIFTI image file
Data collection	The dataset includes neuromelanin-sensitive images and T1w/T2w anatomical images obtained using 3T MRI scanner. 157 healthy individuals participated in data collection (91 adults: M_{age} = 34.47; SD = 12.10; range = 20–64; female = 58.24 %; 66 children/youths: M_{age} = 13.52; SD = 3.75; range = 8–19; female = 45.46 %). All participants had normal or corrected-to-normal vision and hearing and no history of chronic illness or cognitive impairment.
Data source location	*Virginia Tech, Blacksburg, VA 24060*
Data accessibility	Repository name: Open Science Framework. 157 neuromelanin-sensitive image dataset (age: 8–64yrs) Data identification number: DOI 10.17605/OSF.IO/Z49DV Direct URL to data: https://osf.io/z49dv/

1. Value of the Data

- The dataset includes 157 images of neuromelanin-sensitive and anatomical T1w/T2w images, offering significant potential for synergies in brain research focused on exploring the brainstem.
- A standard non-linear neuromelanin-sensitive atlas (1 mm, MNI space) has been generated based on 157 individual images through an iterative warping process. This non-linear template is particularly valuable in addressing the common challenge of a limited field of view (FoV) in neuromelanin-sensitive images.
- The dataset includes a locus coeruleus (LC) probability atlas, addressing the challenge of uncertainty variance depending on the choice of LC atlas. This probability atlas is generated by averaging the individual LC, which is calculated by transforming multiple pre-existing LC atlases to each individual's native neuromelanin space.

2. Background

The overarching objective of the dataset is to foster significant synergies in brain research that seeks to investigate the role of the brainstem in human cognition [1–4]. To this end, the current dataset incorporates neuromelanin-sensitive images from 157 individuals. As a byproduct of norepinephrine metabolism that accumulates in brainstem regions such as the locus coeruleus and substantia nigra, the neuromelanin content in the brain serves as a valuable metric for estimating cognitive functions including as age-related cognitive reservedness and memory performance [5,6]. Furthermore, it has been associated with the onset and progression of neurodegenerative diseases such as Alzheimer's and Parkinson's [7,8]. Neuromelanin values also exhibit a positive correlation with other structural parameters, such as cortical thickness, volume, and microstructure integrity [2]. Hence, the current dataset not only facilitates the visualization and detection of neuromelanin content of the brainstem regions, but also provides valuable resources for investigating the role of the norepinephrine system in human cognition and behavior.

In addition, leveraging individual neuromelanin-sensitive images, the dataset includes a non-linear neuromelanin-sensitive standard atlas (1 mm, MNI space), produced by an iterative sequence of image-processing steps [9–11]. This standard template is particularly beneficial in

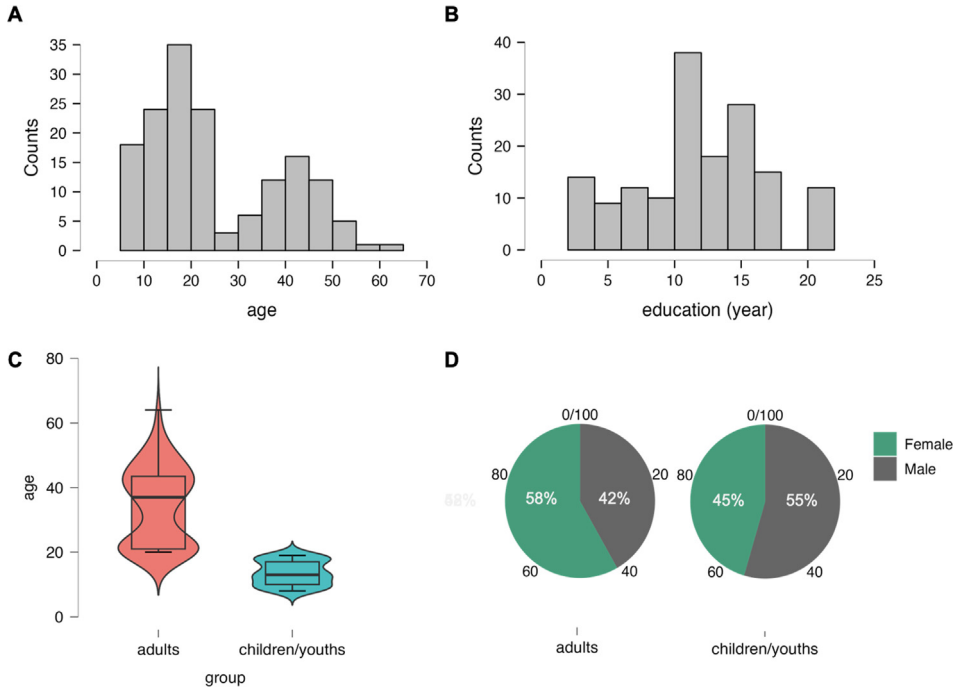

Fig. 1. Basic demographic snapshot of the dataset.

scenarios where the limited field of view (FoV) of neuromelanin-sensitive images presents a common challenge during spatial registration. Finally, the dataset offers a more comprehensive LC probability atlas generated by combining pre-existing multiple atlas-based segmentations on 157 individual neuromelanin-sensitive images.

2.1. Data description

The dataset includes neuromelanin-sensitive images and T1w/T2w anatomical images obtained from 157 healthy individuals. Additionally, a non-linear neuromelanin-sensitive atlas based on the individual neuromelanin-sensitive anatomical images is included. Furthermore, the dataset offers an LC probability atlas, generated using a multi-atlas-based majority voting approach. Before being uploaded to the data repository, all MRI images were defaced using 'fsl_deface' [12] in FSL 6.0.1 [13]. The non-linear neuromelanin-sensitive atlas and LC probability atlas are provided with the following categories: all (N = 157), adults (N = 91), and children/youth (N = 66).

3. Experimental Design, Materials and Methods

3.1. Samples

157 healthy individuals participated in data collection (Fig. 2; 91 adults: M_{age} = 34.47; SD = 12.10; range = 20–64; female = 58.24 %; 66 children/youths: M_{age} = 13.52; SD = 3.75; range = 8–19; female = 45.46 %; Fig. 1 and Table 1). All participants had normal or corrected-to-normal vision and hearing and no history of chronic illness or cognitive impairment. All par-

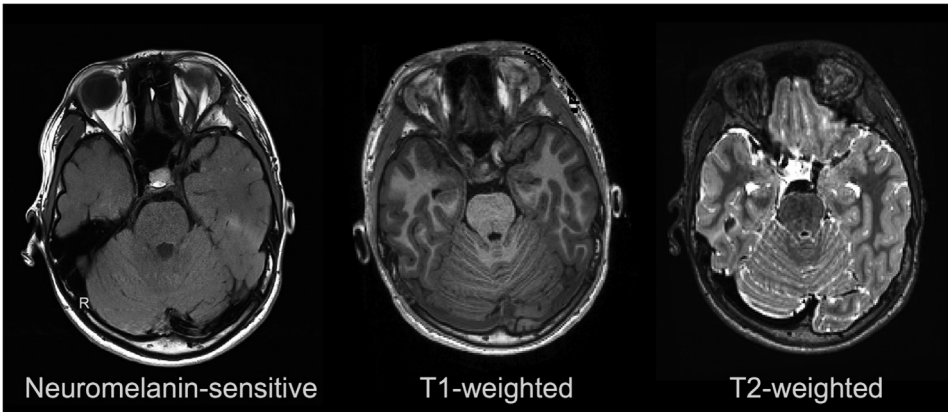

Fig. 2. Image types in the dataset.

Table 1
Basic demographic statistics ($N = 157$).

	Group	Mean	SD	Minimum	Maximum
Age	adults	34.47	12.10	20	64
	Children /youths	13.52	3.75	8	19
Education (years)	adults	15.62	2.98	12	21
	Children /youths	8.23	3.45	3	14
Sex	adults	58.24 % female			
	Children /youths	45.46 % female			

adults $N = 91$; children/youth $N = 66$.

ticipants provided written informed consent approved by the Virginia Tech Institutional Review Board.

3.2. MRI images and acquisition

The neuromelanin-sensitive images were collected through a T1-weighted FSE imaging sequence (T1-FSE) with the following parameters: repetition time, TR = 750 ms, echo time, TE = 12 ms, flip angle = 120°, one average to enhance the signal-to-noise ratio (SNR), 11 axial slices, field of view (FoV) = 220 mm, bandwidth = 285 Hz/Px, slice thickness = 2.5 mm, slice gap = 1.0 mm, and in-plane resolution = 0.43 × 0.43 mm [6,14]. High-resolution T1/T2-weighted anatomical images were collected with the following parameters: T1w–TR = 3200 ms, TE = 2.06 ms, flip angle = 8°, bandwidth = 220 Hz/Px, Fov = 256 mm, voxel resolution = 1 mm^3 isotropic. T2w–TR = 2500 ms, TE = 56 ms, flip angle of 120°, bandwidth of 725 Hz/Px, FoV = 256 mm, voxel resolution of 1 mm^3 isotropic.

3.3. Non-linear neuromelanin-sensitive MNI brain template

To provide a standard neuromelanin-sensitive atlas, we performed an iterative sequence of image-processing steps in which individual neuromelanin-sensitive images were iteratively and non-linearly fitted to a new template generated from the previous iteration [9–11]. Due to the complex structural variability across individuals, a fixed single-brain atlas or a simple linear average atlas may not accurately represent every brain structure. Thus, deformable, nonlinear average brain atlases with reparations can be more elastic in defining anatomical boundaries.

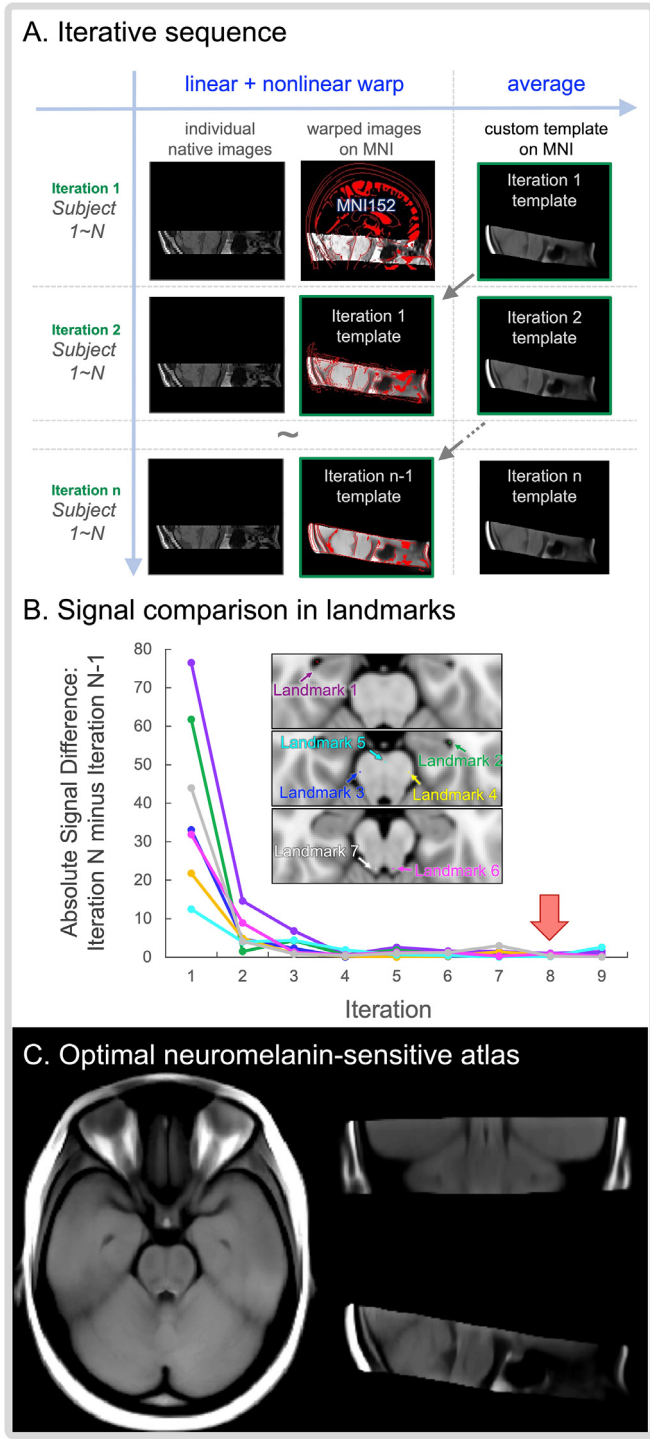

Fig. 3. (A) An iterative sequence of image-processing steps (B) Signal changes between iteration at each landmark (C) Final standard neuromelanin-sensitive atlas.

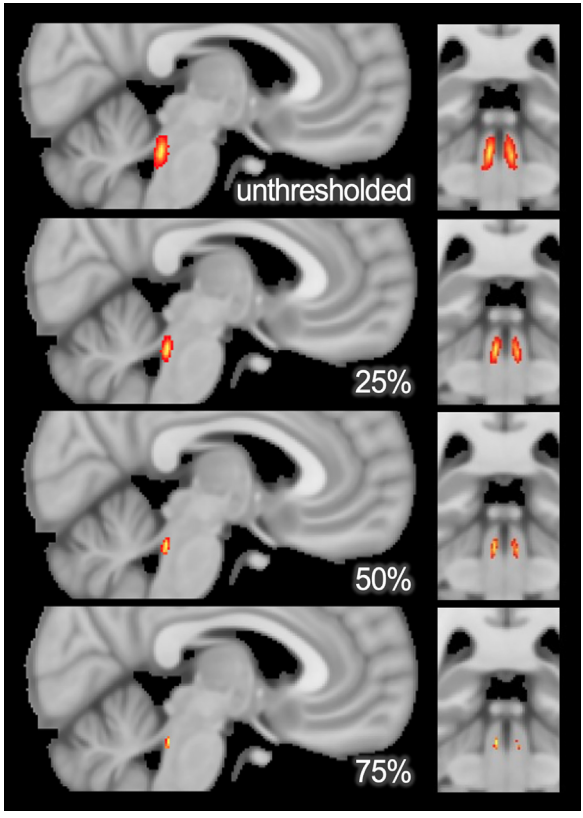

Fig. 4. An atlas of LC with different probability thresholds (unthresholded, 25 %, 50 % and 75 % probability threshold). These probabilities are determined through a majority voting process.

To this end, an affine transformation matrix and a nonlinear warp were first calculated between each individual neuromelanin-sensitive image, individual anatomy image, and MNI 152 template (1 mm). These matrices were then simultaneously applied to native neuromelanin-sensitive images through concatenation, facilitating effective and accurate warping onto the final destination standard space (i.e., MNI 152) with b-spline interpolation. Then, the initial neuromelanin-sensitive template was created by averaging all individuals' warped images (please see 'average' at Iteration 1 in Fig. 4A), prioritizing spatial information over local accuracy, ensuring that the resultant template incorporated MNI space information and comprehensively representing neuromelanin distribution patterns in the studied population. At each iteration, it resulted in improved contrast and definition of landmark locations such as the 4th ventricle area and the boundary of the cerebellum (Fig. 4B) while reducing the variation in the boundary of the LC. This repeated process stopped at iteration 8, where the mean differences between successive iterations were lowest, marking the completion of the template refinement (please see an arrow in Fig. 3B). The final standard atlas shown in Fig. 3C is thus included in the dataset.

3.4. A probabilistic LC atlas based on the segmentation through majority voting from multi-atlases

A majority voting method was implemented to generate an individual LC segmentation from five distinct warped atlas images [15–19]. This approach utilized population probabilities and

maintained the consistency of individual voxel intensities within target regions. To this end, we applied ANTs deformable registration with normalized cross-correlation (2-mm radius, 3-mm smoothing of the deformation map) of joint T1w/T2w (preprocessed: bias-field correction, skull stripping, a rigid transform into the standard MNI brain, and correcting intensity inhomogeneity using N4). Subsequently, individual LC segmentations were completed using five atlases on the neuromelanin-sensitive space. The majority voting method was then applied across five segments using a criterion where the threshold exceeded 50 % probability. The final majority-voted segment of each individual was transformed to the 1mm-MNI space and averaged across 157 individuals, resulting in probability information.

Fig. 4 shows the spatial information of the LC at various thresholds. This probability atlas can mitigate uncertainty variance arising from a single specific template in future studies.

Limitations

Not applicable.

Ethics Statement

All participants provided written informed consent approved by the Virginia Tech Institutional Review Board.

Data Availability

157 neuromelanin-sensitive image dataset (age: 8 - 64yrs) (Original data) (Open Science Framework).

CRediT Author Statement

Tae-Ho Lee: Conceptualization, Supervision, Investigation, Methodology, Formal analysis; **Sun Hyung Kim:** Conceptualization, Methodology, Formal analysis, Visualization; **Benjamin Katz:** Conceptualization; **Il Hwan Kim:** Conceptualization.

Acknowledgements

Grants and funding: This work was done based on research supported by R01AG075000/AG/NIA NIH and by Virginia Tech Lay Nam Chang Dean's Discovery Fund.

Declaration of Competing Interest

The authors declare that they have no known competing financial interests or personal relationships that could have appeared to influence the work reported in this paper.

References

[1] T.-H. Lee, et al., Arousal increases neural gain via the locus coeruleus–noradrenaline system in younger adults but not in older adults, Nat. Hum. Behav. 2 (5) (2018) 356–366.
[2] S.L. Bachman, et al., Locus coeruleus MRI contrast is associated with cortical thickness in older adults, Neurobiol. Aging 100 (2021) 72–82.

[3] M. Mather, C.W. Harley, The locus coeruleus: essential for maintaining cognitive function and the aging brain, Trends Cogn. Sci. 20 (3) (2016) 214–226.
[4] D.V. Clewett, et al., Locus coeruleus activity strengthens prioritized memories under arousal, J. Neurosci. 38 (6) (2018) 1558–1574.
[5] A. Chowdhury, et al., A locus coeruleus-dorsal CA1 dopaminergic circuit modulates memory linking, Neuron 110 (20) (2022) 3374–3388 e8.
[6] D.V. Clewett, et al., Neuromelanin marks the spot: identifying a locus coeruleus biomarker of cognitive reserve in healthy aging, Neurobiol. Aging 37 (2016) 117–126.
[7] P. Olivieri, et al., Early alteration of the locus coeruleus in phenotypic variants of Alzheimer's disease, Ann. Clin. Transl. Neurol. 6 (7) (2019) 1345–1351.
[8] C. Ohtsuka, et al., Changes in substantia nigra and locus coeruleus in patients with early-stage Parkinson's disease using neuromelanin-sensitive MR imaging, Neurosci. Lett. 541 (2013) 93–98.
[9] A.C. Evans, et al., Brain templates and atlases, Neuroimage 62 (2) (2012) 911–922.
[10] V. Fonov, et al., Unbiased average age-appropriate atlases for pediatric studies, Neuroimage 54 (1) (2011) 313–327.
[11] P.M. Thompson, et al., Mathematical/computational challenges in creating deformable and probabilistic atlases of the human brain, Hum. Brain Mapp. 9 (2) (2000) 81–92.
[12] F. Alfaro-Almagro, et al., Image processing and Quality Control for the first 10,000 brain imaging datasets from UK Biobank, Neuroimage 166 (2018) 400–424.
[13] M. Jenkinson, et al., Fsl, Neuroimage 62 (2) (2012) 782–790.
[14] M. Sasaki, et al., Neuromelanin magnetic resonance imaging of locus ceruleus and substantia nigra in Parkinson's disease, Neuroreport 17 (11) (2006) 1215–1218.
[15] B.L. Edlow, et al., Neuroanatomic connectivity of the human ascending arousal system critical to consciousness and its disorders, J. Neuropathol. Exp. Neurol. 71 (6) (2012) 531–546.
[16] N.I. Keren, et al., In vivo mapping of the human locus coeruleus, Neuroimage 47 (4) (2009) 1261–1267.
[17] T. Liebe, et al., In vivo anatomical mapping of human locus coeruleus functional connectivity at 3 T MRI, Hum. Brain Mapp. 41 (8) (2020) 2136–2151.
[18] K.-D. Tona, et al., In vivo visualization of the locus coeruleus in humans: quantifying the test–retest reliability, Brain Struct. Funct. 222 (2017) 4203–4217.
[19] R. Ye, et al., An in vivo probabilistic atlas of the human locus coeruleus at ultra-high field, Neuroimage 225 (2021) 117487.